Recent Results from TRISTAN

Toru Tsuboyama

KEK, National Institute for High Energy Physics
Oho, Tsukuba-shi, Ibaraki-ken, 305 Japan

Abstract

The physics results from the general-purpose spectrometers VENUS, TOPAZ and AMY, at the e^+e^- collider TRISTAN, are presented. Each experiment has accumulated more than 100 pb^{-1} of data at 58 GeV. The detector upgrade programs anticipating increased luminosity are explained. The total and differential cross sections of fermion-pair (μ, τ, hadron-jet, b-quark, c-quark) and $\gamma\gamma$ production are consistent with the Standard Model, and compositeness scales of fermions are excluded up to 2 TeV. The strong-coupling constant is measured using various methods. The contributions from resolved-photon processes in two-photon collisions have been observed for the first time. Finally, the prospects of searches for extra Z bosons and anomalous single-photon events, which are not accessible to experiments on the Z^0 pole, are presented.

Presented at the *Topical conference at the Twentieth SLAC Summer Institute on Particle Physics*, July 13–24, 1992, Stanford, California.

Introduction

The TRISTAN e^+e^- collider, after first collisions in November 1986, has increased its center-of-mass energy to 64 GeV. In 1989, the energy was fixed at 58 GeV and high-luminosity operation with a mini-beta system was started. In November 1991, TRISTAN achieved a luminosity of 1 pb^{-1}/day and, since July 1992, about 140 pb^{-1} of data per experiment have been accumulated. TRISTAN's accumulated luminosity is shown in Fig. 1.

In the energy region of TRISTAN, the interference between photon exchange and Z^0 exchange is nearly maximum; thus, although the cross section is nearly minimum, information on the Standard Model (SM) of electroweak interactions can be derived by careful analyses. The parameters of the SM, which have been precisely determined by the LEP experiments, are now being extrapolated to extremely high energies to select the most favorable GUT model. The measurement of these parameters in the TRISTAN energy region is thus important as an independent piece of information for the extrapolation.

The relatively high luminosity offers fertile sources of $e^+e^- \rightarrow e^+e^-$, $e^+e^- \rightarrow \gamma\gamma$, and two-photon collisions.

Fermion production in this energy region is sensitive to interference effects due to new phenomena: e.g., the presence of extra Z bosons, the compositeness of fermions and $\tilde{e}$ searches through single-photon events. In e^+e^- collisions on the Z pole, the sensitivity to these phenomena is smaller because of the large Z-exchange cross section.

Upgrade of detectors

Three general-purpose solenoidal spectrometers, AMY, TOPAZ and VENUS, have operated stably since the beginning of TRISTAN. For high-luminosity operation, reliable lepton identifiers and vertex detectors are required to study b-quark production, because the B mesons have a lifetime of about 1 ps and their semi-leptonic branching ratio is about 23%. In 1991, VENUS and TOPAZ installed jet-type vertex chambers, and AMY installed a straw chamber. Their operation has already started and the physics analyses are in progress.

The VENUS experiment successfully operated a large-scale Transition Radiation Detector (TRD) [1], with inner and outer diameters of 2.54 m and 3.11 m and a length of 2.96 m, to identify electrons at $|\cos\theta| < 0.7$. The TRD measures the energy of the transition-radiation x-ray that is proportional to the γ value of a charged particle. The performance of the TRD will be presented in a later section.

Small angle calorimeters are getting more important at high luminosities because the statistical error in the luminosity measurement is now so small, and the hermeticity of the calorimetry is required for anomalous-single-photon searches. Each TRISTAN detector installed a new small angle calorimeter (Fig. 2) [2-3]. TOPAZ and AMY measure the electron interaction point by silicon strip detectors, and a systematic error of 1% is expected in the luminosity measurement.

The status of each spectrometer is listed in Table 1.

Table 1. Summary of detector status.

	VENUS	TOPAZ	AMY
Mag. Field	0.75T	1T	3T
Tracker (σ_p/p (%))	Drift Chamber $\sqrt{(0.8pt)^2+(1.3)^2}$	TPC $\sqrt{(1.5pt)^2+(1.6)^2}$	Drift Chamber ($0.6pt$)
Barrel Cal. (σ_E/E @29 GeV))	Pb Glass (3.8%)	Pb Glass (4.5%)	Pb-MWPC (10%)
Endcap Cal.	Liquid Argon	Pb-MWPC	Pb-MWPC
Small Angle Calorimeter	Spaghetti ($\theta > 45$ mr)	BGO + Si ($\theta > 60$ mr)	Pb-Scinti + Si ($\theta > 40$ mr)
Vertex Det.	Jet cell	Jet cell	Straw
Particle ID (hadron)	TOF	TPC (dE/dX)+TOF	
Particle ID (e)	E/p +TRD	E/p+TPC(dE/dX)	E/p
Particle ID (μ)	Muon Chamber	Muon Chamber	Muon Chamber

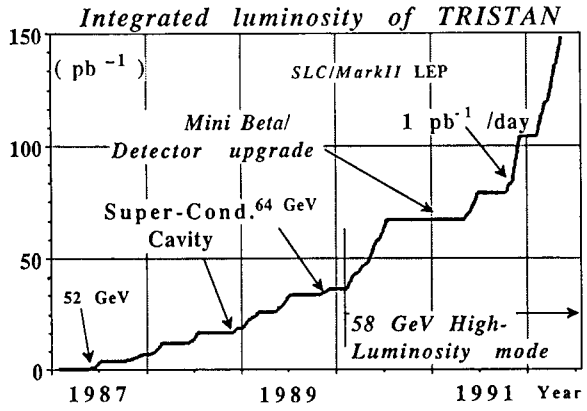

Fig. 1. The luminosity of the TRISTAN accelerator.

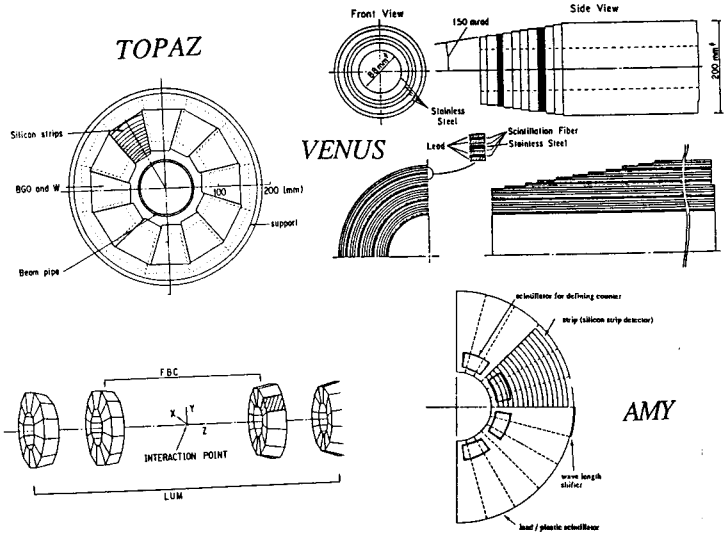

Fig. 2. New small-angle calorimeters.

Fermion-pair and γ-pair production

In this energy region, the contribution of Z^0 exchange becomes substantial and the Standard Model predicts the cross section and asymmetry of lepton production to be $R_{\ell\ell}$ = 1.05 and $A_{\ell\ell}$ = –0.34. The differential cross sections for $ee \to \mu\mu$ and $ee \to \tau\tau$ [4-6] are shown in Fig. 3, and the values of $A_{\ell\ell}$ and $R_{\ell\ell}$ are derived (Table 2). The $A_{\ell\ell}$ values are consistent with the SM prediction. The $R_{\ell\ell}$ values seem to be slightly inconsistent with the SM. The discrepancy is not significant statistically; however, vigorous study of analysis techniques and theoretical calculations are continuing. The differential cross sections of Bhabha scattering are shown in Fig. 4. The differential cross sections of $ee \to q\bar{q}$, measured with the jet-charge method [7-9] are shown in Fig. 5 together with the SM prediction.

Table 2. Asymmetries and R values of lepton production.

Process	Group	Lumi. (pb^{-1})	Result	SM
$ee \to \mu\mu$	VENUS	67.8	R= 1.011±0.033±0.029 A=–0.289±0.034	1.054 –0.338
	TOPAZ	74.0	σ =25.4±0.9±1.2 pb A=–0.322±0.031±0.011	27.4 pb –0.335
	AMY	88.5	R= 0.984±0.032 A=–0.330±0.029	1.056 –0.343
$ee \to \tau\tau$	VENUS	67.8	R= 1.026±0.042±0.035 A=–0.325±0.042	1.054 –0.338
	TOPAZ	74.0	σ =27.1±1.1±1.2 pb A=–0.339±0.049±0.010	27.4 pb –0.335
	AMY	102	R= 1.034±0.035±0.025 A=–0.344±0.031±0.014	1.055 –0.345

Note: AMY updated the results after the conference.

The total and differential cross sections of $ee \to \gamma\gamma$ obtained by VENUS and TOPAZ are shown in Fig. 6 [10-11]. The solid line

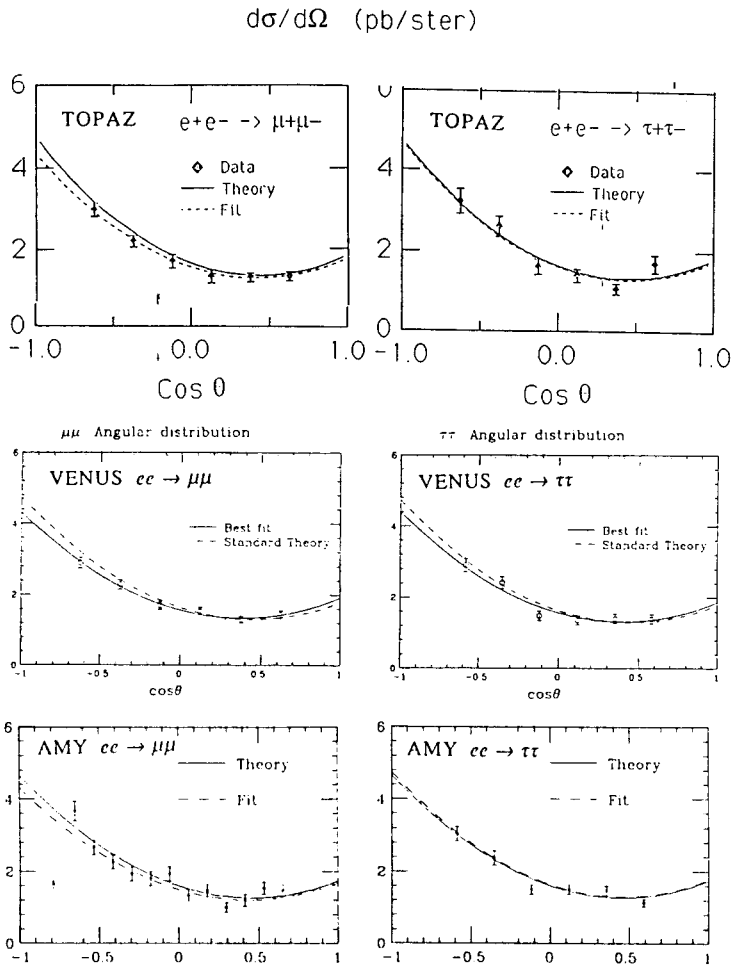

Fig. 3. Differential cross sections of μ-pair and τ-pair production.

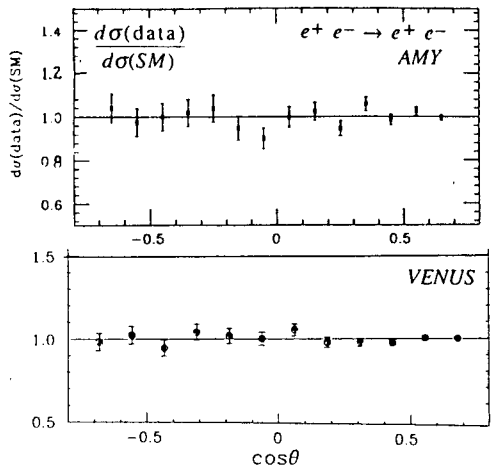

Fig. 4. The differential cross section of Bhabha scattering, normalized by the SM prediction.

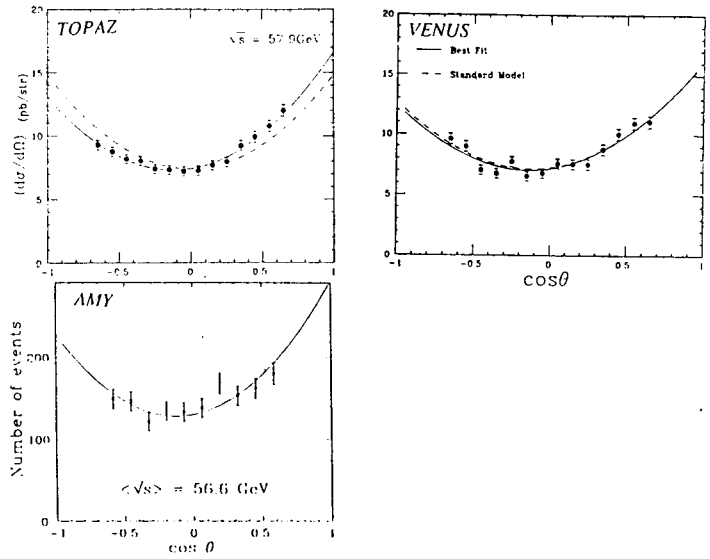

Fig. 5. Jet-charge differential cross sections.

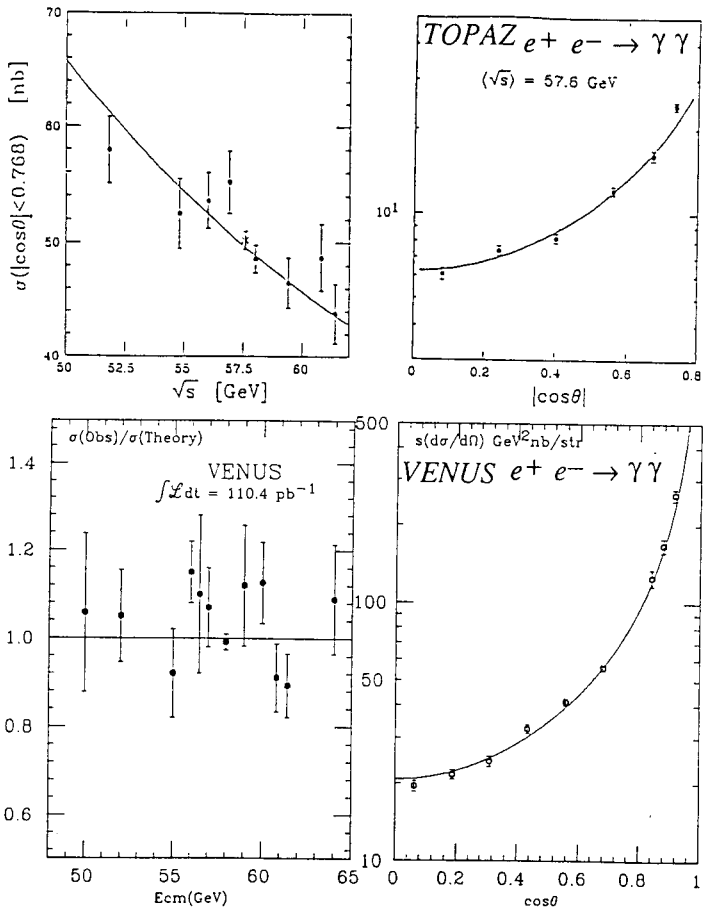

Fig. 6. Total and differential cross sections of $ee \rightarrow \gamma\gamma$.

corresponds to the QED prediction. Consistency between the data and the theory can be confirmed. Recently, L3 at LEP [12] reported an excess of $ee \rightarrow \mu\mu\gamma\gamma$ and $ee \rightarrow ee\gamma\gamma$ events with $M\gamma\gamma$ = 58 GeV, however, no anomaly is observed for the $\gamma\gamma$ final state in the TRISTAN energy region: $52 < \sqrt{s} < 64$ GeV.

Asymmetry of *b* and *c* quarks

The c- and b-quark jets can be identified by using their semi-leptonic decay. In the VENUS detector a TRD [1] was installed in 1991 and it improved the electron-identification capability. Figure 7 shows the distribution of x-ray energy. A pion-rejection efficiency of 95% is achieved at an electron-detection efficiency of 80%. Figure 8 shows the E/p distribution after the TRD requirement. The resulting electron purity is more than 90% even though electrons are included in hadron jets. Thus, not only high-p_t electrons in b-quark jets but also low-p_t electrons in c-quark jets can be identified. A combined fit of differential cross sections in the high-p_t and low-p_t regions is made (Fig. 9), and the b-quark and c-quark asymmetries are obtained simultaneously.

The decay mode $D^{*\pm} \rightarrow D^0\pi^{\pm}$, on the other hand, enables us to reconstruct D^* mesons [13]. Figure 10 shows the $\Delta M = M(\pi D) - M(D)$ distribution for $D \rightarrow \pi K$, $\pi\pi K$ and $\pi\pi\pi K$, obtained by VENUS. A clear peak can be seen for $\Delta M = 145$ MeV/c^2 corresponding to D^* production. The purity is estimated to be 70%. Using this sample, the asymmetry of c-quark production is obtained.

Since the Q value of this decay mode is 5.8 MeV, the π momentum in the rest frame of the D^* is 40 MeV/c. The distribution of p_t^2 with respect to the jet axis is shown in Fig. 11. The enhancement at $p_t^2 \sim 0$ corresponds to π's from D^* decay. The excess of events is estimated by fitting a background function and a signal function. The contributions from the D^* are

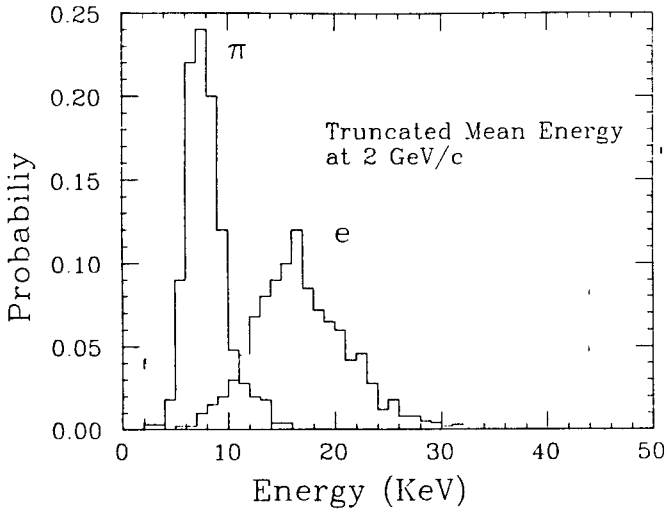

Fig. 7. X-ray energy distribution measured by the VENUS TRD.

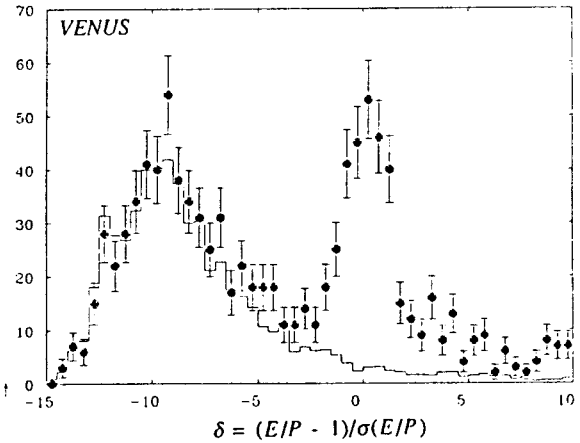

Fig. 8. E/p distribution by VENUS. The plots show the data after the electron identification by the TRD, the histogram shows the π background. The excess of events around $\delta = 0$ corresponds to the electron signal.

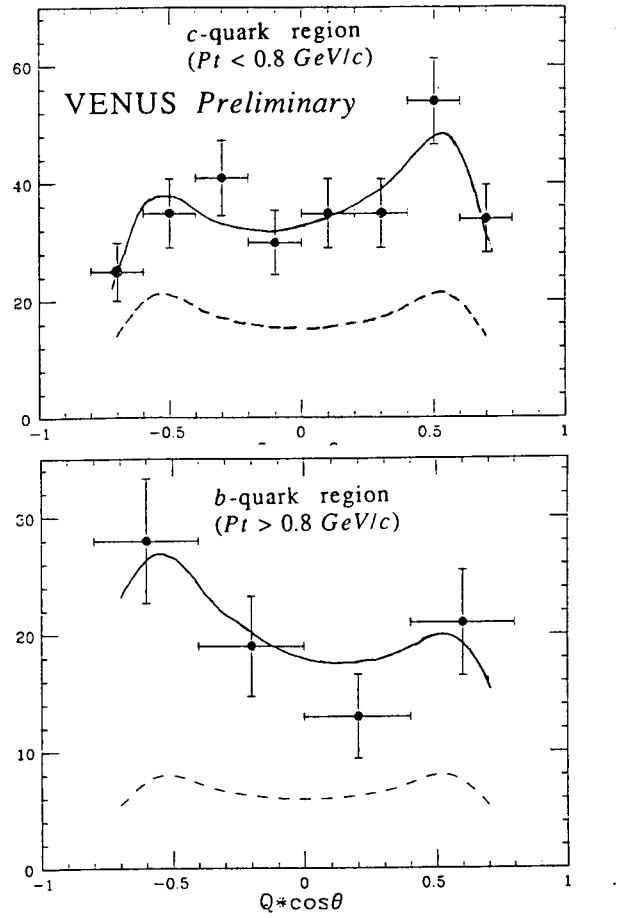

Fig. 9. Combined fit of c- and b-quark angular distribution by VENUS. Flavor is tagged by low-p_t electrons (c-quark) and low-p_t electrons (b-quark). The solid line shows the fit result, the dashed line shows the contribution from backgrounds.

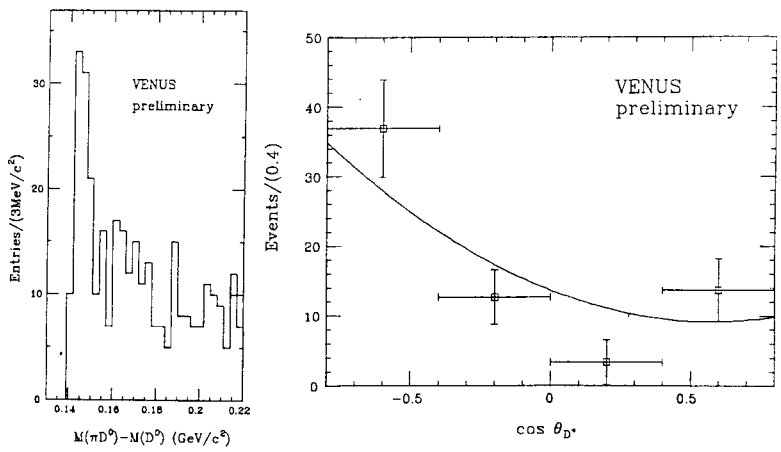

Fig 10. The $\Delta M = M(\pi D) - M(D)$ distribution (left), and the event angular distribution in the D^* region (right).

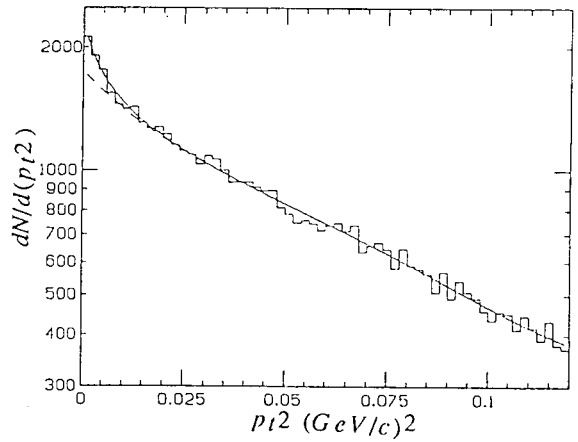

Fig. 11. The particle p_t^2 distribution from the jet axis. The dashed line is an extrapolation of background function, the enhancement of events at $p_t^2 < 0.025$ $(\mathrm{GeV}/c)^2$ corresponds to pions from D^*.

estimated in the forward and backward regions, and the charge asymmetry is extracted. The purity is lower than for the above two methods; however, the good statistics make this method useful.

The results thus obtained are listed in Table 3 together with previous TRISTAN results [13-17]. For b-quark asymmetry, $B^0\bar{B}^0$ mixing plays an important role. The $B_d\bar{B}_d$ mixing (χ_d) has been measured by CLEO and ARGUS, however, the $B_s\bar{B}_s$ mixing (χ_s) is ambiguous. A precise measurement of b-quark asymmetry can constrain the χ_s value, although, the statistical level of the TRISTAN experiments is not enough to give a constraint on χ_s.

Table 3. $e^+e^- \rightarrow q\bar{q}$ asymmetry ($<\sqrt{s}>=58$ GeV).

		Asymmetry	Lumi. (pb^{-1})	SM (**)	Tagging
Average	VENUS	0.099±0.016±0.018	65	0.089	jet charge
	TOPAZ	0.091±0.014±0.016	46	0.090	jet charge
	AMY	0.083±0.029±0.019	27	0.087	jet charge
c-quark	VENUS	−0.43±0.14±0.04(*)	113	−0.47	$\Delta M = M(D^*) - M(D)$
		−0.45±0.12(*)	113		soft pion: D^*
		−0.37±0.22	50		low-p_t e : TRD
b-quark	VENUS	−0.59±0.21±0.06	66	−0.58	high-p_t e: E/p
		−0.55±0.28(*)	50		high-p_t e: TRD
		−0.50±0.22±0.06	61		μ detector
	TOPAZ	−0.54±0.25±0.07	44	−0.58	high-p_t e: E/p
		−0.71±0.34±0.07	41		μ chamber
	AMY	−0.82±0.25±0.14	33	−0.58	high-p_t μ
		R-value			
b-quark	TOPAZ	0.81±0.18±0.08	44	0.56	high-p_t e: E/p
		0.59±0.15	41		μ chamber
	AMY	0.47±0.12±0.10	33	0.56	μ chamber

(*) Preliminary, systematic error is under study.

(**) The effect of $B^0\bar{B}^0$ mixing is not corrected for in the SM predictions.

Compositeness scales of fermions

Since fermion production in the TRISTAN energy region is found to be well described by the SM, the compositeness scale of

hypothetical four-fermion contact interactions, *eeff*, where *f* is *e*, μ, τ or *q*, can be derived from the differential cross sections. From the $ee \rightarrow \gamma\gamma$ process, similar compositeness scales of the $ee\gamma\gamma$ coupling can be derived. The results are shown in Table 4. Compositeness scale up to about 2 TeV is excluded by the TRISTAN experiments.

Table 4. Lower bounds of Contact-interactions scale parameters $ee \rightarrow$ fermion-pair (unit = TeV, 95% C.L.).

Process	Group	Lumi	LL		RR		VV		AA	
		(pb^{-1})	Λ+	Λ−	Λ+	Λ−	Λ+	Λ−	Λ+	Λ−
$ee \rightarrow \mu\mu$	VENUS	27.3	1.6	2.0	1.6	2.0	3.2	3.0	2.2	4.1
	TOPAZ	74.0	2.3	2.0	2.4	2.1	–	2.9	3.0	4.6
$ee \rightarrow \tau\tau$	VENUS	27.3	1.8	1.3	1.8	1.3	3.2	2.5	2.4	2.4
	TOPAZ	74.0	2.5	2.2	2.6	2.3	3.9	3.2	2.8	2.8
$ee \rightarrow ee$	VENUS	69.6	1.2	1.9	1.2	1.8	3.5	3.1	2.9	2.5
	AMY	80	2.6	2.5	2.6	2.5	4.8	6.2	1.7	4.4
$ee \rightarrow qq$	VENUS	65	1.0	2.1	1.9	2.4	3.6	3.0	4.1	5.3
	TOPAZ	46.1	1.2	1.6	2.8	3.3	4.9	4.5	6.2	7.2

$ee \rightarrow \gamma\gamma$ (Unit=GeV, 95% C.L.)

Group	Lumi	L,R		L+R		L−R
	(pb^{-1})	Λ+	Λ−	Λ+	Λ−	Λ+,Λ−
VENUS	110	155	71	186	85	66
TOPAZ	50	102	89	121	105	65
AMY		68	69	81	82	52

Determination of the QCD-coupling constant

The QCD-coupling constant, α_S, is measured precisely by the LEP experiments. It is, however, still meaningful to verify the running feature. The value of α_S can be determined directly from the total hadronic cross section. The model dependence is small, however, its sensitivity to α_S is not enough to overcome the ambiguities in the radiative corrections and luminosity measurement. On the other hand, the shape analysis is less dependent on luminosity measurement and radiative corrections if the model dependence is reasonably understood.

AMY [18] measured the coupling in various ways based on a data sample of about 60 pb^{-1} (Fig. 12). The Monte Carlo generators based on the $O(\alpha_S{}^2)$ Matrix Element (*ME*) [19] and on the Next-to-Leading-Log approximation (*NLL*) [20] are used. The following shape parameters are studied: Energy-Energy Correlation (*EEC*), its asymmetry (*AEEC*) and jet-multiplicity (three-jet ratio or differential jet multiplicity).

VENUS [18] measured the differential jet ratio and obtained $\Lambda_{\overline{MS}} = 237 \pm 25 \pm 30$ MeV based on the *NLL* generator. If the results are extrapolated to the Z^0 pole, they are consistent with $\alpha s(Mz)$ values measured by LEP experiments. The result from VENUS is shown in Fig. 13.

Gluon Properties

(1) Three-gluon coupling

The jet structure of hadronic final states was first observed at SPEAR and gluon production was subsequently confirmed in three-jet events by PETRA experiments. In the TRISTAN energy region the three-gluon coupling (non-Abelian nature) is established through analysis of four-jet events as follows. The diagrams for four-jet final states are shown in Fig. 14, where the last diagram corresponds to the three-gluon coupling. The angular correlations among the four jets, χ_{BZ} and $\cos\theta_{NR}$ (Fig. 15), were investigated to extract the three-gluon coupling. The first attempt was made by AMY [21]. By performing similar analyses, VENUS obtained limits on the group parameters [22], and the Abelian gluon model is excluded at 95% C.L. Recently, TOPAZ measured χ_{BZ} and $\cos\theta_{NR}$ with 120 pb^{-1} of data (Fig. 16). The results of Monte Carlo simulations with the three-gluon coupling *on* and *off* are also plotted. It is clear that the parton shower model with a three-gluon coupling explains the data best.

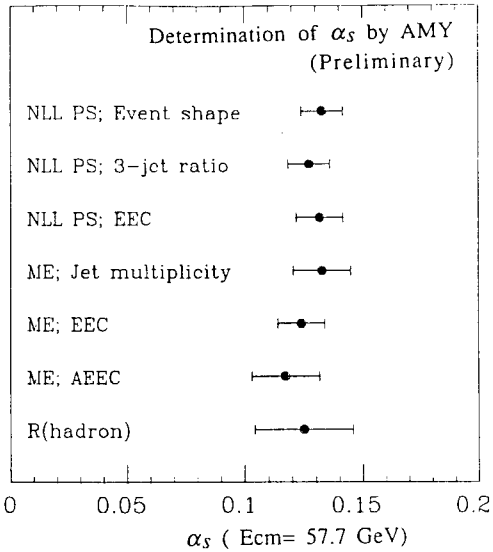

Fig. 12. Strong coupling constant measured by AMY.

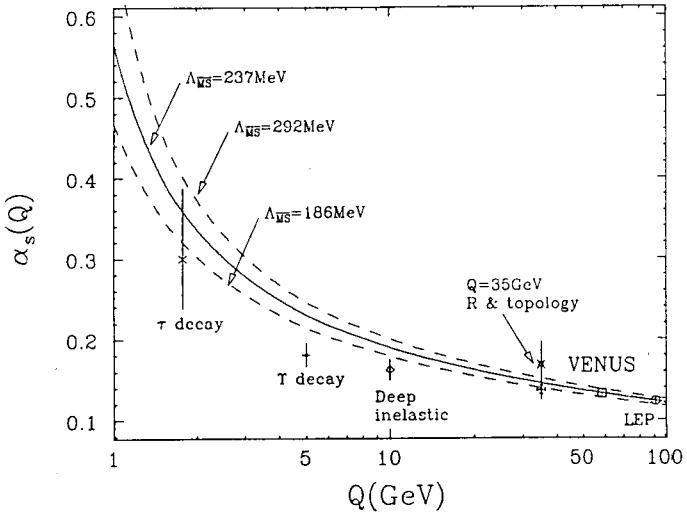

Fig. 13. The running feature of α_S (VENUS).

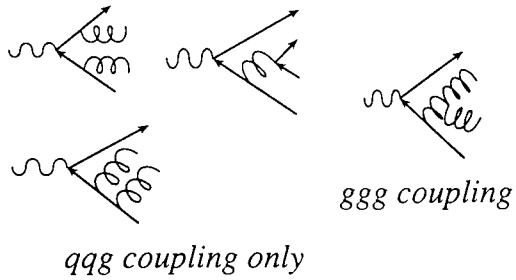

Fig. 14. Lowest-order diagrams for four-jet final states. The diagram on the right corresponds to the three-gluon coupling.

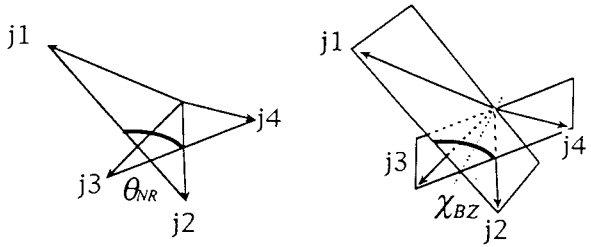

Fig. 15. The definition of angles θNR and χBZ.

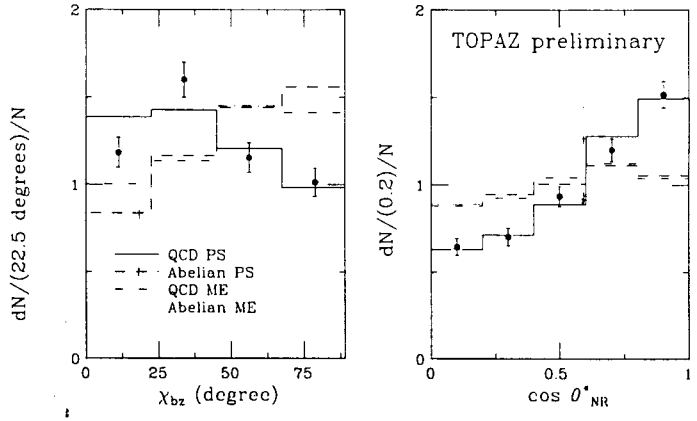

Fig. 16 The distributions of $\cos\theta NR$ and χBZ measured by TOPAZ.

(2) Difference between gluon jets and quark jets

The difference between quark jets and gluon jets has been an important issue. AMY collected three-jet events, [23]. Assuming that the jet with the smallest energy comes from a gluon (gluon-enriched jet), jet properties are studied. As an example, the distribution of ξ, the energy fraction of particles in a cone having $\theta < 60° / \sqrt{E_{jet}}$, for gluon-enriched jets is shown in Fig. 17. The predictions by the JETSET parton-shower model [24] and the JETSET matrix element model with the independent fragmentation scheme of Hoyer *et al.*, [25] ($q=g$ model) are shown. Clearly, the PS model represents the data well. The enhancement of events at low ξ implies that gluon jets are fatter than quark jets.

VENUS made an inclusive analysis [18]. To obtain the gluon-containing events, they collected three-jet events whose final-state jets approximate an equilateral triangle. They are assumed to be the $e^+e^- \to q\bar{q}g$ sample. For the quark-jet sample, two-jet events with a hard initial-state radiation, $e^+e^- \to q\bar{q}\gamma$, are used. These events are also required to make an equilateral triangle. Because of energy-momentum conservation, hadron jets in both final states have equal energy: $\sim \sqrt{s}/3$. In Fig. 18, the ratio of distributions of the fractional particle-momentum distribution, $X_p = p/E(\text{jet})$, is plotted. A clear deviation from one is observed, and it indicates the difference between jet properties of qqg and $qq\gamma$ events. Here also the JETSET parton shower model [24] fits the data best. The enhancement of particles in the lower X_p region indicates that gluons tend to produce low-momentum particles.

Two-photon processes

In the TRISTAN energy region, the s-channel cross section is still much smaller than that at the Z-pole, while the cross section for two-photon collisions is slowly increasing. In addition, the separation between s-channel processes and two-photon

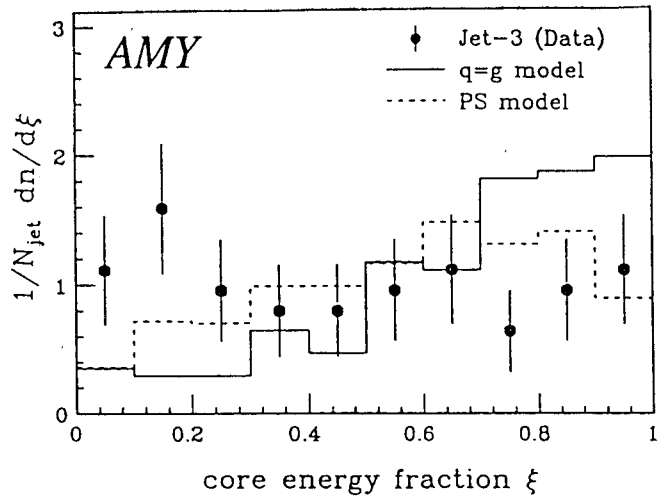

Fig. 17. The distribution of core-energy fraction for gluon-enriched events by AMY.

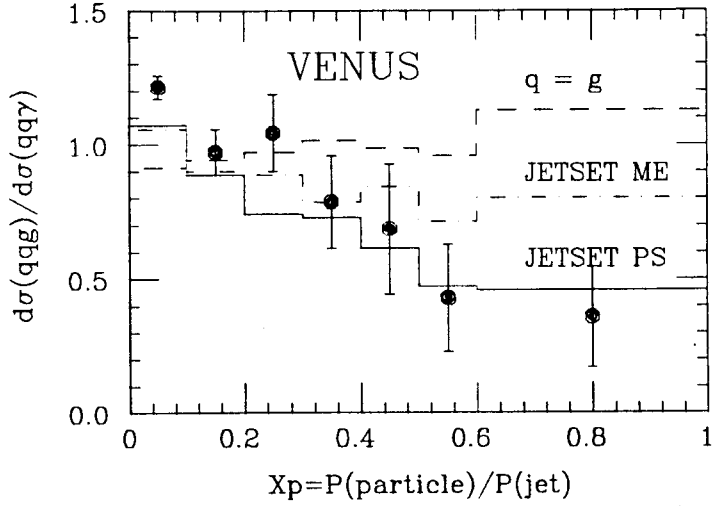

Fig. 18. The ratio of fractional-momentum distributions for the qqg events and $qq\gamma$ events by VENUS.

processes becomes clearer as the center-of-mass energy goes up. Therefore, the TRISTAN region is an ideal place to study two-photon collisions.

(1) $f_2(1270)$ meson

The $f_2(1270)$ meson has been analyzed by TOPAZ and VENUS. Its decay width to the $\gamma\gamma$ state, $\Gamma(f_2 \rightarrow \gamma\gamma)$, provides information on resonance models. The f_2 production is identified by the decay $f_2 \rightarrow \pi^+\pi^-$. TOPAZ [26] made a fit to the $\pi^+\pi^-$ invariant mass spectrum and obtained $\Gamma(f_2 \rightarrow \gamma\gamma)$ to be 2.27 ± 0.47 ± 0.11 keV. VENUS measured the differential cross section for $\gamma\gamma \rightarrow \pi^+\pi^-$ and made a partial-wave analysis. The states of spin 0, 1 and 2 are included and a value of $\Gamma(f_2 \rightarrow \gamma\gamma)$ of 2.5 ± 0.5 keV is obtained. The evaluation of the systematic error is now in progress. The results are shown in Fig. 19 together with previous results.

(2) Hadronic-structure function of the photon (f_2)

The hadronic-structure of the photon can be probed by using single-tagged two-photon hadronic events. It is found by Kapsta [27] that f_2 is not sensitive to Λ_{QCD} but that it can be phenomenologically explained by the sum of f_2(QCD:uds), f_2(QPM:cb) and f_2(VDM). A cut on the p_t of the spectator quark, $p_t{}^0$, is introduced to separate the contributions from the point-like part and hadronic part. The f_2 value is measured up to $Q^2 \sim$ 300 GeV^2 by TRISTAN experiments [28-29]. The f_2 value averaged over $0.3 < x < 0.8$ is shown as a function of Q^2 in Fig. 20. The data favor a small value of $p_t{}^0$. The increase of f_2 in the large Q^2 region indicates the validity of the model by Kapsta.

(3) Confirmation of resolved-photon processes

In the TRISTAN energy region, the total cross section of *no* tagged $ee \rightarrow ee +$ *hadron* events is larger than the predictions by the QPM and the VDM. Recently, Drees and Godbole [30] calculated the contributions of "resolved photons" shown in Fig.

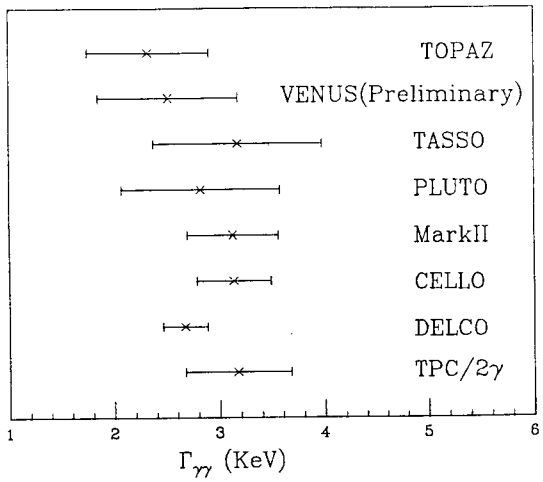

Fig. 19. $\Gamma(f_2 \rightarrow \gamma\gamma)$ measured by VENUS and TOPAZ, together with previous data.

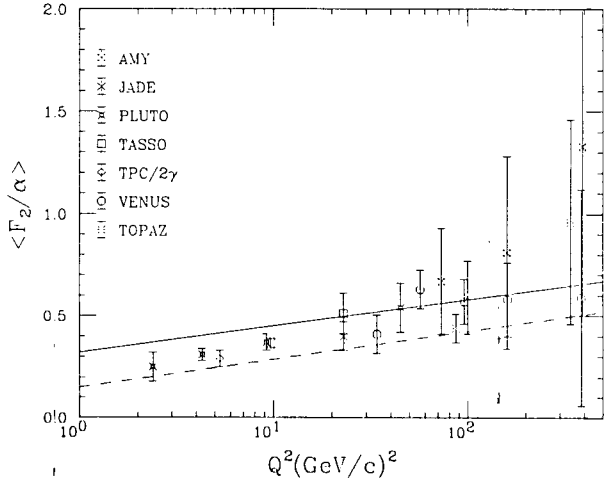

Fig. 20. The f_2 value average over $0.3 < x < 0.8$ as a function of Q^2. Contributions from $c\bar{c}$ and $b\bar{b}$ are subtracted. The solid (dashed) line corresponds to the prediction with $p_t{}^0$ = 0.1 (1.0) GeV.

21. In the resolved case, the final state contains both high-p_t jets and low-p_t spectator jets. The contribution of this process is thought to be a significant background in future linear colliders, thus, precise study of this phenomenon at TRISTAN is important. AMY and TOPAZ [29, 31] analyzed their data to examine this effect. Figures 22(a) and 22(b) show the distribution of p_t (jet). The data in the high-p_t(jet) region cannot be explained without the resolved process. After the selection of p_t (jet) > 3.0 GeV/c, (1.6 GeV/c TOPAZ) the thrust distribution, calculated in the center-of-mass system of the hadronic particles, is shown in Fig. 22(c) and (d). There is good agreement between the data and the prediction including the resolved process.

Search for new particles

So far, we have not found any significant deviation from the SM. We thus can set limits on new phenomena.

(1) Extra Z bosons

The total hadronic and leptonic cross sections are sensitive to the existence of extra Z bosons. The sensitivity extends above the established Z^0 peak because at TRISTAN the total cross section is small enough and the luminosity is high enough to detect interference effects due to extra Z bosons. For experiments at the Z pole, the large cross section prevents this kind of analysis. On the basis of the E_6 GUT model, a combined fit to R_{qq} and $R_{\ell\ell}$ was made by VENUS [32]. Lower mass limits on ψ, η and χ mesons were obtained to be $M\psi > 125$, $M\eta > 125$ and $M\chi > 231$ GeV/c^2 at 90% C.L. The lower mass limit on a Z_1 boson whose couplings to quarks and leptons are the same as those of the standard Z, is $M(Z_1) > 426$ GeV/c^2 at 90% C.L. Recently, CDF [33] measured the e^+e^- invariant-mass spectrum, and they set a lower limit on the Z_1 mass to be $M(Z_1) > 412$ GeV/c^2 at 95% C.L.

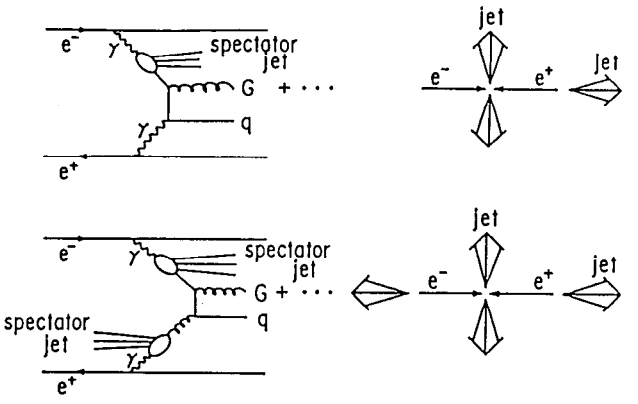

Fig. 21. Diagrams for "resolved proccesses" of photon-photon collisions (right); their event configurations (left) [25].

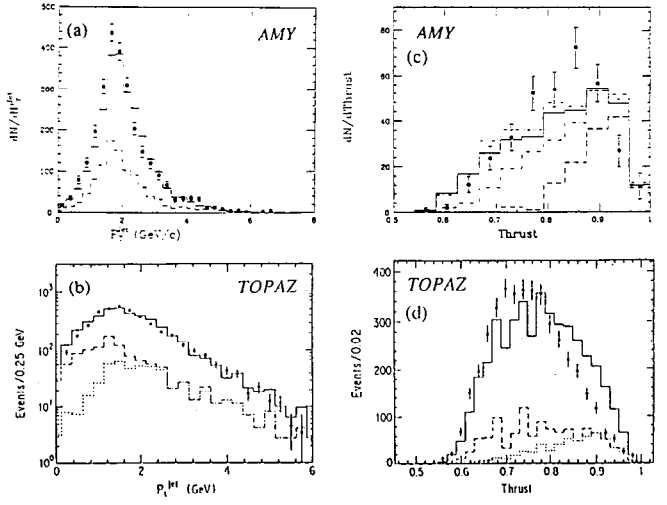

Fig. 22. (a) and (b) The p_t(jet) distributions. 22(c) and (d) Thrust distributions for $p_t^{jet} > 3.0$ GeV/c (AMY) and 1.6 GeV/c (TOPAZ). The predictions of VDM, VDM + QPM and VDM + QPM + "resolved process" are shown by the dotted, dashed and solid lines.

(2) Scalar electrons

Single-photon events, in which only one high-p_t γ is observed, offer a unique probe of the production of new weakly interacting particles in reactions such as $e^+e^- \rightarrow \gamma\tilde{\gamma}\tilde{\gamma}$. In the SM, single-photon events are explained by $e^+e^- \rightarrow \gamma\nu\bar{\nu}$. Small-angle radiative Bhabha events are vetoed by small angle calorimeters. The VENUS experiment updated their single-photon measurement [34] using 61 pb^{-1} of data. After applying the criteria θ_{veto} = 5° and $p_t > 0.18\ Ebeam$, one event is observed, while the SM predicts 1.86 events. The cross section contribution from additional processes is less than 0.073 pb at 90% C.L., and the limits on $\tilde{e}$ and $\tilde{\gamma}$ shown in Fig. 23 are obtained. The lower-mass limit for the $\tilde{e}$ is found to be 41.5 GeV/c^2 assuming a massless $\tilde{\gamma}$ and the mass degeneracy of left-handed and right-handed $\tilde{e}$'s. The TRISTAN groups installed new small-angle calorimeters in order to improve their veto angle. For VENUS, with 300 pb^{-1} of luminosity, the sensitivity to scalar electrons exceeds 80 GeV/c^2 which will not be accessible even to LEP200 experiments where the $e^+e^- \rightarrow \bar{\nu}\nu\gamma$ process dominates the final state.

Summary

The TRISTAN accelerator has achieved a luminosity of 1 pb^{-1}/*day* at a center-of-mass energy of 58 GeV. The detectors have been upgraded successfully to meet the requirements of high-luminosity precision physics. The fermion-production channels are consistent with the Standard Model. A slight inconsistency exists, especially in the total cross sections. Careful comparisons are required in theoretical calculations as well as in experimental and analysis techniques. However, the compositeness-scales of fermions are excluded up to 2 TeV. TRISTAN is one of the best sources of two-photon collisions, and various insights on hadron resonances and photon structures

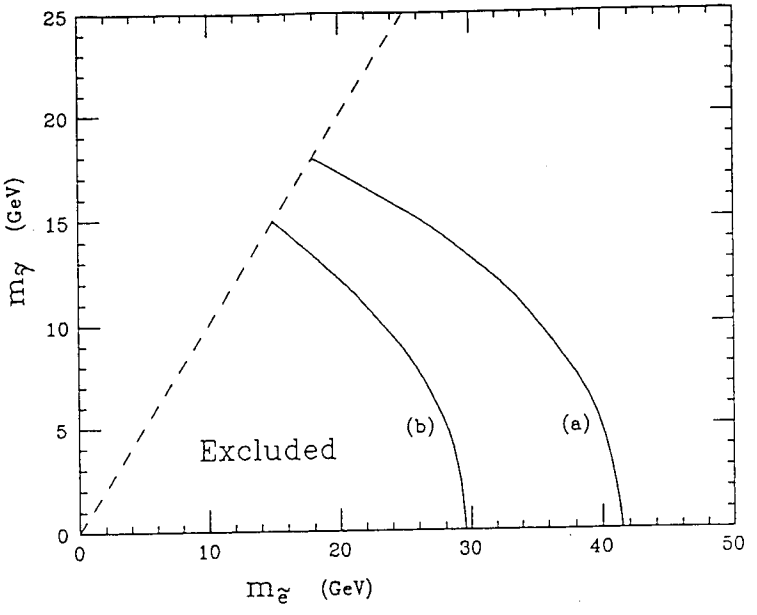

Fig. 23. The $\tilde{e}$ and $\tilde{\gamma}$ region excluded by VENUS at 90% C.L. The contour (a) shows non-degenerate $\tilde{e}$, and (b) shows degenerate case.

have been obtained. The potential of TRISTAN for new particle searches is illustrated by the results on extra Z bosons and supersymmetric electrons.

Acknowledgments

The present talk is based on data from the AMY, TOPAZ and VENUS experiments at the TRISTAN e+e– collider. The author thanks the people who provided the data, and the TRISTAN Accelerator Group. He also wishes to thank the organizers of the SLAC Summer Institute for inviting him to the Topical Conference, and for interesting and pleasant meetings.

References

[1] M. Sakuda *et al.*, Nucl. Instrum. Meth. A311, 57 (1992).

[2] H. Hayashii *et al.*, Nucl. Instrum. Meth. A316, 202 (1992).

[3] F. Takasaki *et al.*, KEK-Preprint-91-58 (1991), *unpublished.*

[4] A. Bacala *et al.*, Phys. Lett. B218, 112 (1989).

[5] K. Abe *et al.*, Z. Phys. C48, 13 (1990).

[6] B. Howell *et al.*, Phys. Lett. B291, 206 (1992).

[7] K. Abe *et al.*, Phys. Lett. B232, 425 (1989).

[8] D. Stuart *et al.*, Phys. Rev. Lett. 64, 983 (1990).

[9] I. Adachi *et al.*, Phys. Lett. B255, 613 (1991).

[10] K. Abe *et al.*, Z. Phys. C45, 175 (1989).

[11] K. Shimozawa *et al.*, Phys. Lett. B284, 144 (1992).

[12] L3 Collaboration, CERN-PPE/92-152 (1992).

[13] A. Okamoto *et al.*, Phys. Lett. B278, 393 (1992).

[14] M. Shirakata *et al.*, Phys. Lett. B278, 499 (1992).

[15] H. Sagawa *et al.*, Phys. Rev. Lett. 63, 2341 (1989).

[16] K. Nagai *et al.*, Phys. Lett. B278, 506 (1992).

[17] A. Shimonaka *et al.*, Phys. Lett. B268, 457 (1991).

[18] Proceedings of the Second KEK Topical Conference on e^+e^- Collision Physics, KEK, Tsukuba, Japan (1991).

[19] R. K. Ellis, D. A. Ross, and A. E. Terrano, Nucl. Phys B178, 421 (1981).

[20] K. Kato and T. Munehisa, Phys. Rev. D36, 61 (1987); K. Kato and T. Munehisa, Phys. Rev. D39, 156 (1989).

[21] I. H. Park *et al.*, Phys. Rev. Lett. 62, 1713 (1989).

[22] K. Abe *et al.*, Phys. Rev. Lett. 66, 280 (1991).

[23] Y. K. Kim *et al.*, Phys. Rev. Lett. 63, 1772 (1989).

[24] M. Bengtsson and T. Sjostrand, Nucl. Phys. B289, 810 (1987).

[25] P. Hoyer *et al.*, Nucl. Phys. B161, 349 (1979).

[26] I. Adachi *et al.*, Phys. Lett. B234, 185 (1990).

[27] K. Kapsta, Z. Phys. C42, 225 (1989).

[28] T. Sasaki *et al.*, Phys. Lett. B252, 491 (1990).

[29] H. Hayashii, The Ninth International Workshop on Photon-Photon Collisions, San Diego (1992), NWU-HEP 92-03 (1992).

[30] M. Drees and R. M. Godbole, Nucl. Phys. B339, 355 (1990).

[31] R. Tanaka *et al.*, Phys. Lett. B277, 215 (1992).

[32] K. Abe *et al.*, Phys. Lett. B246, 297 (1990).

[33] F. Abe *et al.*, Phys. Rev. Lett. 68, 1463 (1992).

[34] K. Abe *et al.*, Phys. Lett. B232, 431 (1989).